Electronic Supplementary Material (ESI) for Journal of Materials Chemistry A.

Supporting Information

Achieving Performance and Longevity with Butane-operated Low-temperature Solid Oxide Fuel Cells using Low-Cost Cu and CeO_2 Catalysts

Cam-Anh Thieu, Sungeun Yang, Ho-Il Ji, Hyoungchul Kim, Kyung Joong Yoon, Jong-Ho Lee, and Ji-Won Son**

Table S1. Metal prices on 02 August 2021[1]

Metal	Price [$/kg]
Ni	19.9
Cu	9.7
Ru	24,113.1
Pd	86,614.1
Pt	34,144.1

Table S2. Fuel compositions used for SOFC testing

SCR	**C_4H_{10} [%]**	**Steam**		**H_2 [%]**	**N_2 [%]**
		[%]	**°C**		
3	5	60	86.2	5	30
2.5	5	50	81.6	5	40
2	5	40	76.1	5	50

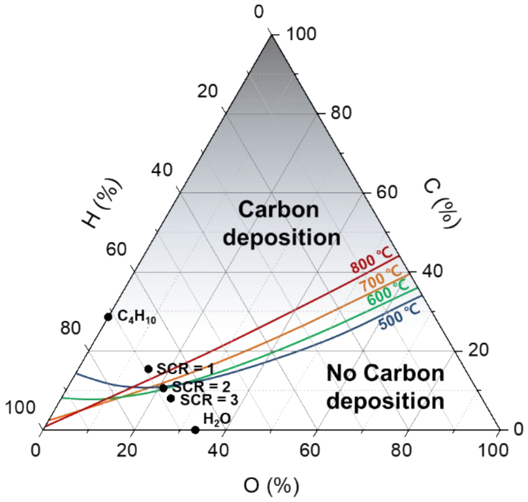

Figure S1. Carbon deposition limits in a C H O ternary diagram calculated at different temperatures and under 1 atm.[2, 3]

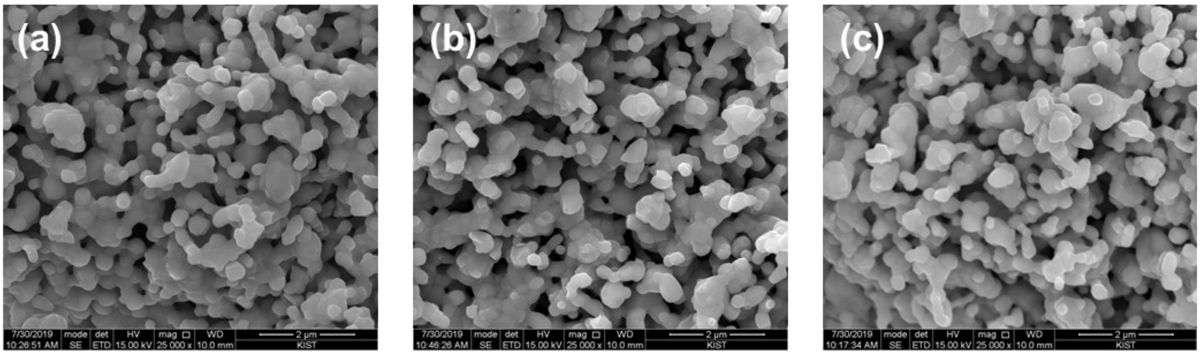

Figure S2. SEM images showing the microstructures of (a) NiO-YSZ powder, (b) Cu-Ni-YSZ powder, and (c) Ce-Ni-YSZ powder

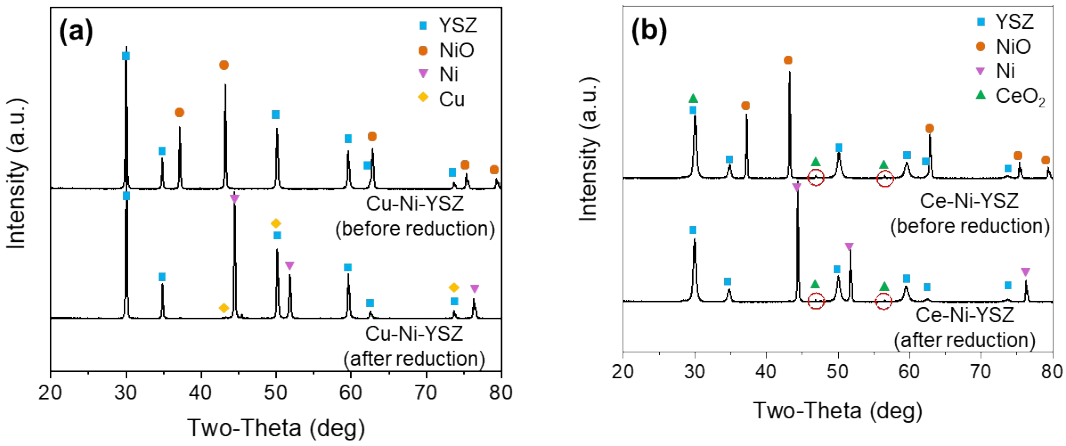

Figure S3. XRD patterns obtained from (a) Cu-Ni-YSZ-powder and (b) Ce-Ni-YSZ powder before and after the reduction treatment.

Table S3. BET surface areas (S_{BET}) of the fabricated catalyst powders post-annealed before reduction

Powder	**S_{BET} (m^2/g)**
NiO–YSZ	4.10 ± 0.13
Cu-Ni-YSZ (Cu infiltrated NiO-YSZ)	4.12 ± 0.15
Ce-Ni-YSZ (Ce infiltrated NiO-YSZ)	4.09 ± 0.12

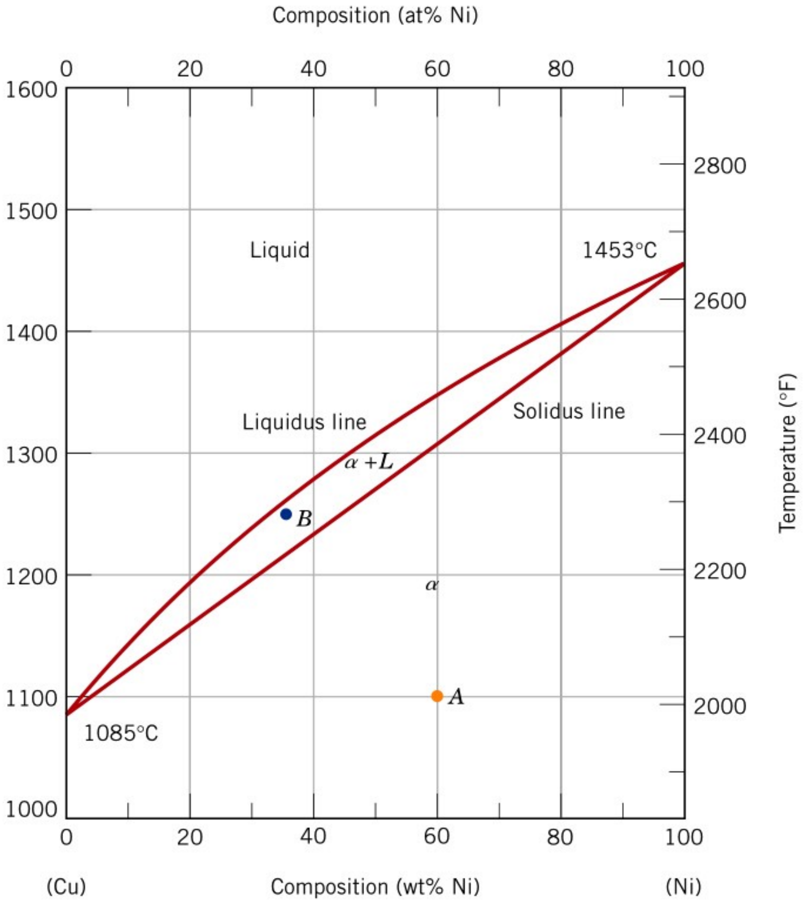

Figure S4. Binary alloy phase diagram of the Cu–Ni system.[4]

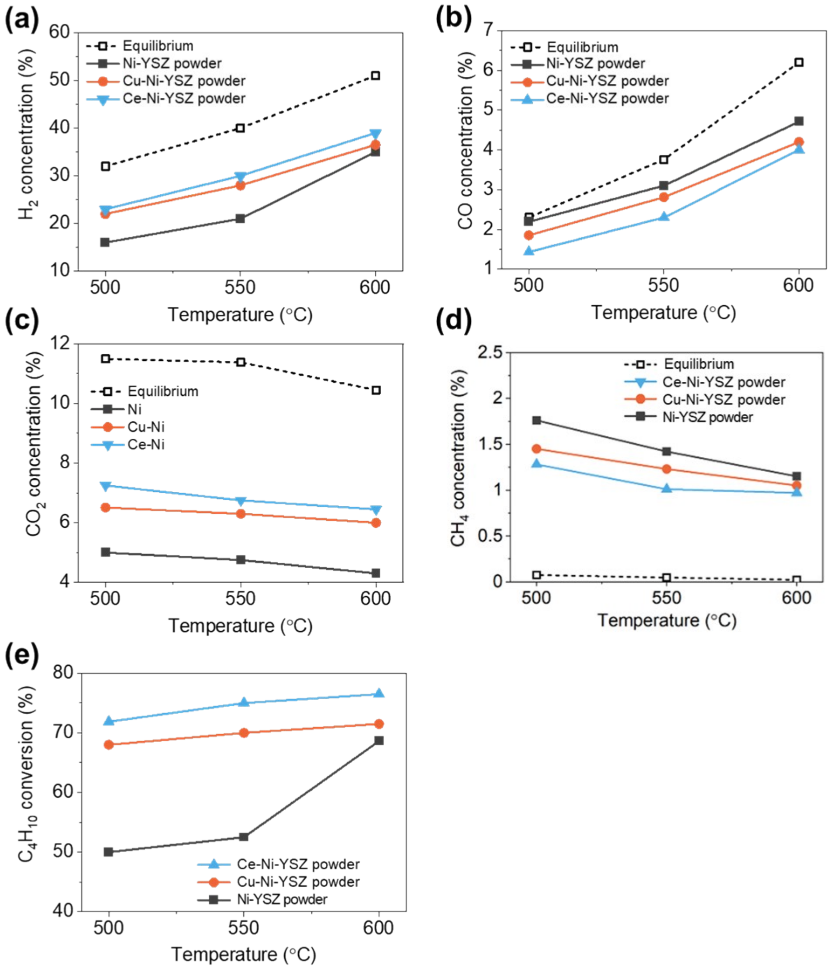

Figure S5. Comparison between the experimentally produced and thermodynamically calculated (a) H_2, (b) CO, (c) CO_2, and (d) CH_4 concentrations (dry basis) as a function of temperature and (e) C_4H_{10} conversion using the experimentally calculated H_2 production.

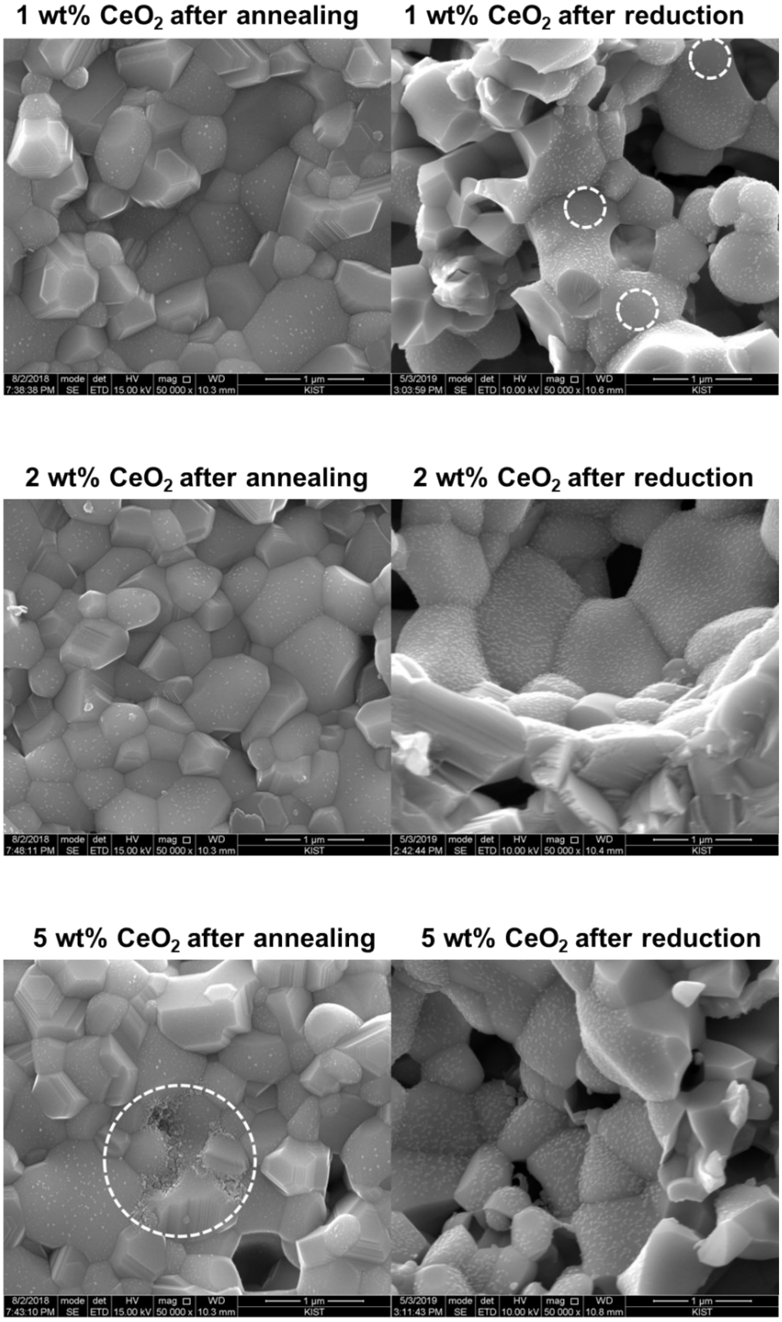

Figure S6. SEM images of anode support region with different amount of CeO_2 infiltration. After post annealing at 650 °C (NiO-YSZ, left) and after reduction at 600 °C (Ni-YSZ, right).

Analyses of the TF-SOFC cell performance over humidified H_2 fuel

The TF-SOFC I–V–P curves from 500 to 650 °C under humidified H_2 were investigated and are shown in Figure S7(note that the I–V–P of the Cu-cell, which was obtained in an earlier study,[5] is plotted together with the obtained data), and the comparison of the I–V–P curves of these cells at 600 °C is shown in Figure S8(a). The open-circuit voltages (OCVs) of the fabricated TF-SOFCs were approximately 1.1 V, which are proper OCV values for TF-SOFCs and reveal that the TF electrolyte was deposited with microstructural integrity. These I–V–P results indicate that the output performance of the Ref-cell and Cu-cell under humidified H_2 does not differ much, whereas the Ce-cell appears to exhibit a slightly better performance than the other two cells. The peak power densities (PPDs) of each cell at different temperatures are listed in Table S3. In particular, the Cu-Ce-cell exhibited the best cell performance among these TF-SOFCs. More specifically, the PPDs at different operating temperatures can be listed in the following order: Cu-Ce-cell > Ce-cell > Cu-cell ~ Ref-cell. Based on this result, it can be postulated that CeO_2 infiltration at the AS enhances the cell performance under humidified H_2. The PPDs were 1.31 W cm^{-2}, 1.33 W cm^{-2},[5] 1.46 W cm^{-2}, and 1.70 W cm^{-2} for the Ref-cell, Cu-cell, Ce-cell, and Cu-Ce-cell, respectively. The results show that the PPDs of the Ce- and Cu-Ce-cell increased by 12 % and 30 %, respectively, when compared with the Ref-cell.

Table S4. PPDs of the fabricated TF-SOFCs at various temperatures over humidified H_2 fuel

Temperature [°C]	**TF-SOFC**	**Peak power density** [mW cm^{-2}]
650	Ref-cell	1740
	Cu-cell	1830
	Ce-cell	2095
	Cu-Ce-cell	2250
600	Ref-cell	1310
	Cu-cell	1330 [5]
	Ce-cell	1460
	Cu-Ce-cell	1700
550	Ref-cell	798
	Cu-cell	828
	Ce-cell	824
	Cu-Ce-cell	1097
500	Ref-cell	403
	Cu-cell	365
	Ce-cell	359
	Cu-Ce-cell	530

EIS plots, including Nyquist and Bode plots, of the fabricated TF-SOFCs under humidified H_2 fuel at 600 °C under OCV conditions is shown in Figure S8(b)–(c), respectively. All the TF-SOFCs demonstrated an identical Ohmic area specific resistance (ASR), which is an expected result if the cell configuration, excluding the catalysts, is identical and there is no significant contact issue in the cell test setup. The polarization ASR (R_P) noticeably decreases with catalyst insertion, and the relative order of the R_P of the TF-SOFCs is Cu-Ce-cell < Ce-cell < Cu-cell < Ref-cell. The smaller R_P of the cells containing CeO_2 clearly indicates better electrode performance, which results in better cell performance.

The contribution of the various electrode processes (with different relaxation times) to the polarization ASR, R_P, can be identified and evaluated by EIS deconvolution and interpretation. The distribution of relaxation time (DRT) is a recently developed method. The plots of the regularization parameter, γ(freq.), vs. log[freq.] of the fabricated TF-SOFCs at 600 °C under humidified H_2 fuel are shown in Figure S9. According to the results, five distinctive peaks can be clearly identified, which are in accordance with an earlier report.[5] The area of each peak corresponds to its major elementary process in the electrochemical reaction. The corresponding relationship between the characteristic peaks and electrode processes can be described as follows and in Table S4:

(i) The peak in the frequency range of 10^0–10^1 Hz (P1), as shown in Figure S10(a), shows a negligible operating-temperature dependency. Hence, it may be related to the mass transfer process caused by the gas-phase diffusion in the pores of the Ni-YSZ anode substrate because the cathode in our system is very thin (a few microns), but the anode is thick owing to the anode-supported cell configuration.

As shown in Figure S9, for the Cu-cell, multilayer deposition during the Cu insertion in the AFL facilitated gas diffusion to a certain extent due to opening of the YSZ network during the fabrication process. The Ce- and Cu-Ce-cell with CeO_2 enrichment at the interface enhanced the triple phase boundary and increased the number of catalytically active sites for fuel gas oxidation, leading to an improvement in the gas-phase diffusion. Thus, the P1 process is sensitive to the modified electrodes when catalysts are inserted. The order of the trend is as follows: Ref-cell > Cu-cell ~ Ce-cell > Cu-Ce-cell.

(ii) The peak in the frequency range of 10^4–10^5 Hz (P4) is also independent of the temperature (Figure S10(a)) and shows negligible sensitivity to the catalyst material (Figure S9). The peak in this frequency range is associated with ohmic resistance of fuel electrode[6] or charge transfer reaction at the triple phase boundary.[7] However, those two mechanisms are highly affected by the temperature. Therefore, further study is needed to clarify the exact process related to this peak.

(iii) The peak in the frequency range of 10^3–10^4 Hz (P3) may correspond to the charge exchange reactions at the anode and cathode and the electrolyte interfaces. It is shown in Figure S10 (b) that the P3 peak is slightly dependent on the operating temperature. In addition, it can be observed in Figure S9 that the Cu-cell shows negligible dependence on charge transfer because there is no significant difference in the reactive sites (i.e., TPBs); however, the P3 peaks of the Ce-cell and Cu-Ce-cell slightly changed owing to the effect of CeO_2 infiltration. It is clear from this result that the infiltration of CeO_2 into the Ni-YSZ anode results in the reduction of the activation energy for the anodic charge transfer reaction, leading to improved electrode reactions.

(iv) The peaks in the frequency range of 10^1–10^3 Hz (P2 and P2’) are considered to correspond to the reaction mechanism related to the electrode process. The P2’ peak of the Cu-Ce-cell is considerably smaller than that of the Ce-cell, Cu-cell, and Ref-cell, indicating the infiltration of CeO_2 is effective in reducing the resistance of the TPB reaction at the anode side. The primary reason is that the presence of CeO_2 nanoparticles at the AS affords an extension of the O^{2-} conducting domain into the electronic conducting domain and promotes oxidation of the H_2 molecules.[8, 9]

Table S5. Cell processes identified by DRT analysis and physical meanings

Process	**Frequency range** [Hz]	**Dependencies**	**Physical meaning**
P1	10^0–10^1	Catalyst insertion	Gas-phase diffusion
P2	10^1–10^2	Temp., catalyst insertion	Related-electrode reaction
P2’	10^2–10^3	Temp., catalyst insertion	Related-electrode reaction
P3	10^3–10^4	Temp., catalyst insertion	Charge-transfer reaction
P4	10^4–10^5	Independent	Insensitive factor

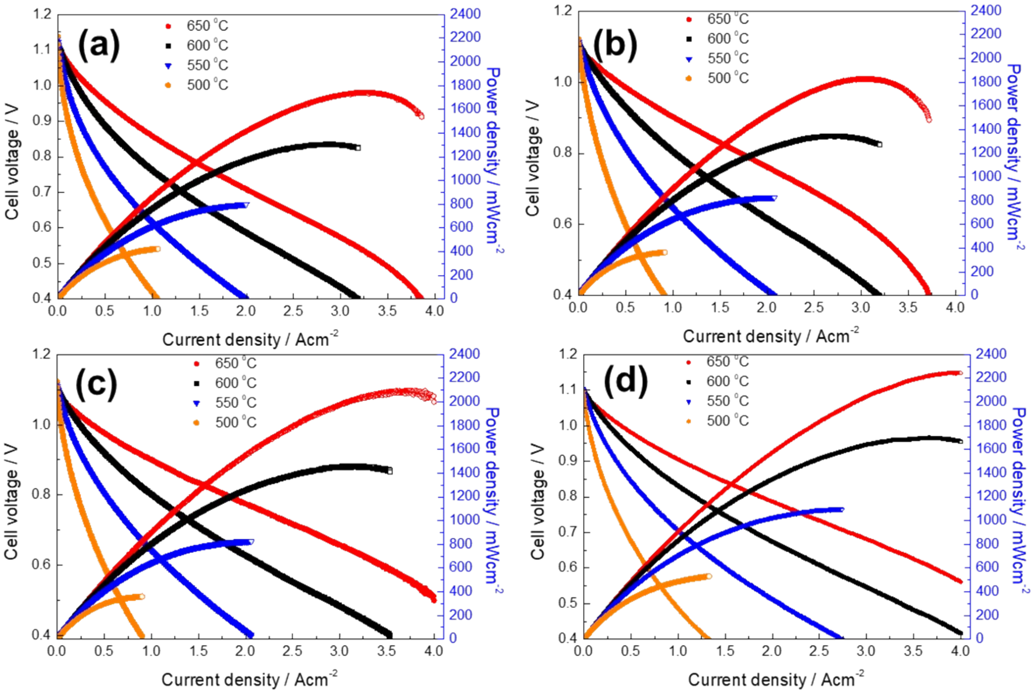

Figure S7. I–V–P curves of the (a) Ref-cell, (b) Cu-cell, (c) Ce-cell, and (d) Cu-Ce-cell under humidified H_2 fuel with a temperature range of 500–650 °C. The I–V–P curve of the Cu-cell at 600 °C reported in an earlier study[5] was plotted together with the experimental data.

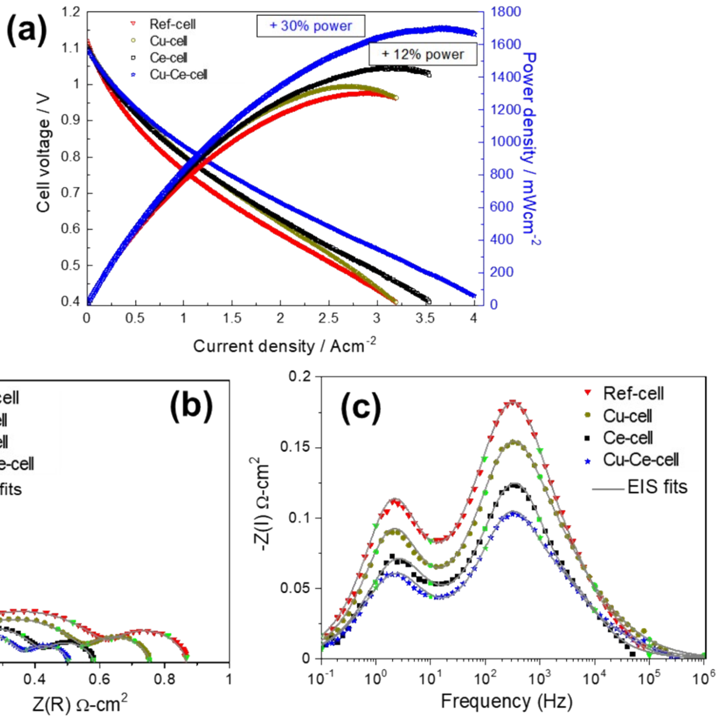

Figure S8. (a) I–V–P curves, (b) Nyquist plots, and (c) Bode plots at OCV conditions of the fabricated TF-SOFCs under humidified H_2 fuel at 600 °C. The I–V–P curve of the Cu-cell at 600 °C procured in an earlier study[5] was plotted together with the experimental data.

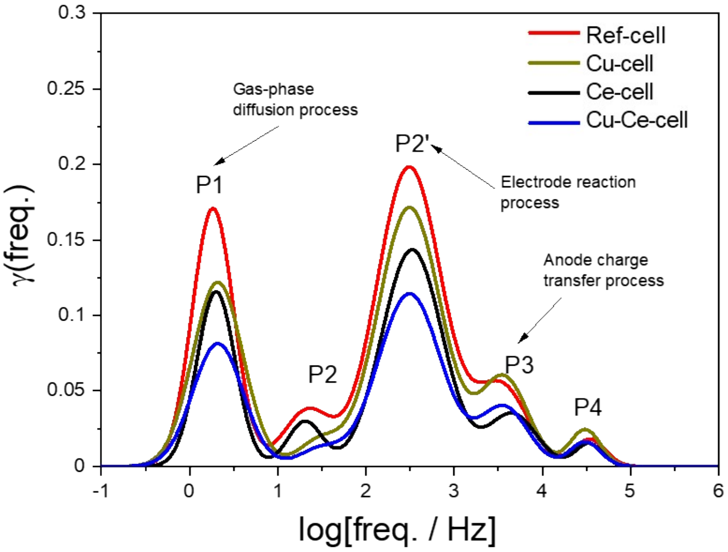

Figure S9. Comparison of the DRT results of the TF-SOFCs at 600 °C under H_2 fuel.

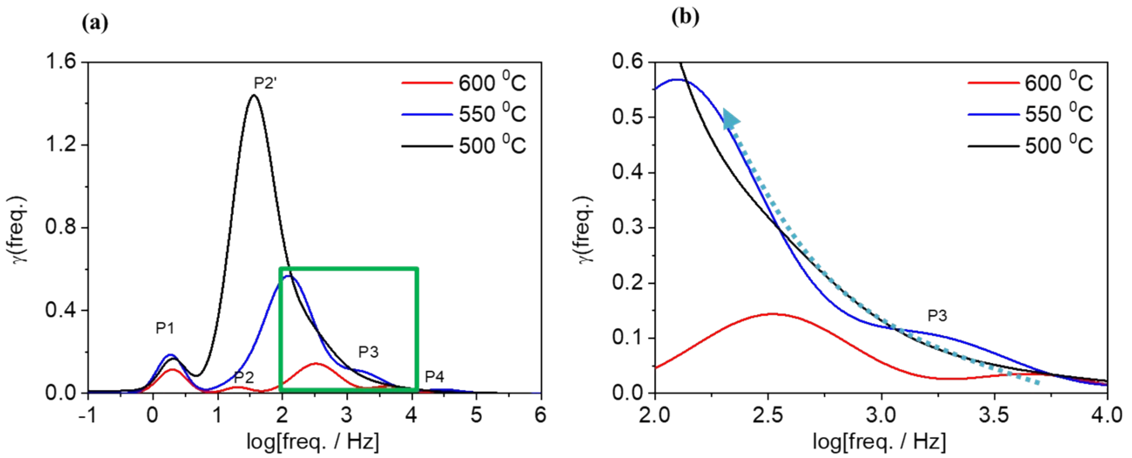

Figure S10. (a) DRT results as functions of the operating temperatures obtained by using the Ce-cell as a unit cell and H_2 as a fuel, and (b) high magnification of the green square in (a) showing the increase of P3.

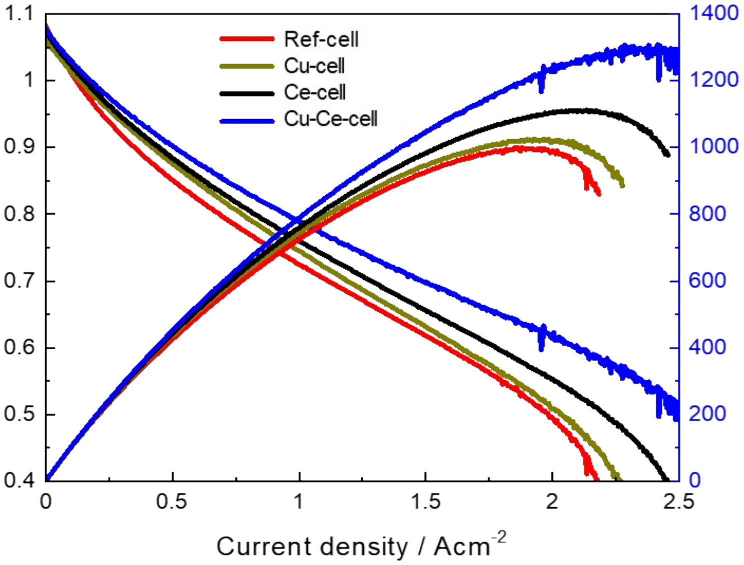

Figure S11. I–V–P curves of the TF-SOFCs at 600 °C with a 50 vol. % H_2 concentration.

Table S6. State-of-the-art internal hydrocarbon reforming SOFCs operating at 700 °C.

Strategy	Cell	Peak power density (W cm^{-2}) at given temperature (°C)					Fuel	SCR or O:C	Durability test			Ref.
		500	550	600	650	700			Operating hours (h)	Degradation (%)	Degradation rate (%/h)	
Alloying and oxide addition	CeO_2-Cu-Ni/YSZ	0.35	0.68	1.12			*n*-butane	3	250	2.76	0.011	This work
Alloying	Ru-Ni-YSZ	0.3	0.59	0.97			*n*-butane	3	100	10	0.1	5
	Pd-Ni-YSZ			0.95			*n*-butane	3	100	14.44	0.14	10
	Sn-Ni-GDC				0.93		dry CH_4	0	40	2.73	0.068	11
	Sn-Ni-SDC (2)			0.28	0.44	0.61	dry CH_4	0	72	1.55	0.022	12
	Ru-Ni-GDC (2)			0.75			dry CH_4	0	n.a.			13
	Ni-Cu-SDC			0.32			dry CH_4	0	12	2	0.17	14
Catalyst layer	$RuNiCeO_X$/Ni-BZCYYb	0.37					wet CH_4	0.036	380	n.a.		15
	Ru-CeO_X/Ni-SDC			0.65			5 % iso-octane–9 % air–3 % H_2O–83 % CO_2	4.32 (O:C)	n.a.			16
	Ru-SDC/Ni-SDC				0.46		wet CH_4	0.03	n.a.			17
	$CuMnO_X$-SDC/Ni-SDC			0.17	0.30	0.38	wet CH_4	0.03	80	14.88	0.19	18
Oxide addition	LaO_X-Ni-SDC	0.19	0.36	0.55			wet CH_4	0.03	8	9.75	1.22	19
	CaO_X-Ni-SDC	0.08	0.19	0.43	0.70	1.05	wet CH_4	0	70	10.61	0.15	20

References

[1] Daily Metal Prices, https://www.dailymetalprice.com/metalprices.php, accessed: August, **2021**.

[2] Z. Jaworski, B. Zakrzewska, P. Pianko-Oprych, On thermodynamic equilibrium of carbon deposition from gaseous C-H-O mixtures: updating for nanotubes, Reviews in Chemical Engineering, 33 (2017) 217-235.

[3] K. Sasaki, Y. Teraoka, Equilibria in fuel cell gases - II. The C-H-O ternary diagrams, J Electrochem Soc, 150 (2003) A885-A888.

[4] H. Okamoto, M. E. Schlesinger, E. M. Mueller, ASM Handbook Volume 3: Alloy Phase Diagrams, ASM International, Ohio, 2016.

[5] C.-A. Thieu, S. Yang, H.-I. Ji, H. Kim, K.J. Yoon, J.-H. Lee, J.-W. Son, Effect of secondary metal catalysts on butane internal steam reforming operation of thin-film solid oxide fuel cells at 500–600 °C, Applied Catalysis B: Environmental, 263 (2020) 118349.

[6] J. Hong, A. Bhardwaj, H. Bae, I.-H. Kim and S.-J. Song, Electrochemical Impedance Analysis of SOFC with Transmission Line Model Using Distribution of Relaxation Times (DRT) J Electrochem Soc, 167 (2020) 114504

[7] A. Leonide, V. Sonn, A. Weber and E. Ivers-Tiffée, Evaluation and Modeling of the Cell Resistance in Anode-Supported Solid Oxide Fuel Cells, *J Electrochem Soc*, 155 (2008) B36-B41.

[8] B. Timurkutluk, C. Timurkutluk, M.D. Mat, Y. Kaplan, Anode-supported solid oxide fuel cells with ion conductor infiltration, International Journal of Energy Research, 35 (2011) 1048-1055.

[9] S.P. Jiang, S. Zhang, Y.D. Zhen, A.P. Koh, Performance of GDC-Impregnated Ni Anodes of SOFCs, Electrochemical and Solid-State Letters, 7 (2004) A282.

[10] C.-A. Thieu, S. Park, H. Kim, H.-I. Ji, J.-H. Lee, K.J. Yoon, S. Yang, J.-W. Son, Improved electrochemical performance and durability of butane-operating low-temperature solid oxide fuel cell through palladium infiltration, International Journal of Energy Research, 44 (2020) 9995.

[11] J.-H. Myung, S.-D. Kim, T.H. Shin, D. Lee, J.T.S. Irvine, J. Moon, S.-H. Hyun, Nano-composite structural Ni–Sn alloy anodes for high performance and durability of direct methane-fueled SOFCs, J Mater Chem A, 3 (2015) 13801-13806.

[12] P. Li, Z. Wang, X. Yao, N. Hou, L. Fan, T. Gan, Y. Zhao, Y. Li, J.W. Schwank, Effect of Sn addition on improving the stability of Ni-Ce0.8Sm0.2O1.9 anode material for solid oxide fuel cells fed with dry CH4, Catalysis Today, 330 (2019) 209-216.

[13] T. Hibino, A. Hashimoto, M. Yano, M. Suzuki, M. Sano, Ru-catalyzed anode materials for direct hydrocarbon SOFCs, Electrochim. Acta, 48 (2003) 2531-2537.

[14] Z. Wang, W. Weng, K. Cheng, P. Du, G. Shen, G. Han, Catalytic modification of Ni–Sm-doped ceria anodes with copper for direct utilization of dry methane in low-temperature solid oxide fuel cells, Journal of Power Sources, 179 (2008) 541-546.

[15] Y. Chen, B. deGlee, Y. Tang, Z. Wang, B. Zhao, Y. Wei, L. Zhang, S. Yoo, K. Pei, J.H. Kim, Y. Ding, P. Hu, F.F. Tao, M. Liu, A robust fuel cell operated on nearly dry methane at 500 °C enabled by synergistic thermal catalysis and electrocatalysis, Nature Energy, 3 (2018) 1042-1050.

[16] C. Sun, Z. Xie, C. Xia, H. Li, L. Chen, Investigations of mesoporous CeO2–Ru as a reforming catalyst layer for solid oxide fuel cells, Electrochem. Commun., 8 (2006) 833-838.

[17] K. Wang, R. Ran, Z. Shao, Methane-fueled IT-SOFCs with facile in situ inorganic templating synthesized mesoporous Sm0.2Ce0.8O1.9 as catalytic layer, Journal of Power Sources, 170 (2007) 251-258.

[18] C. Jin, C. Yang, H. Zheng, F. Chen, Intermediate temperature solid oxide fuel cells with Cu1.3Mn1.7O4 internal reforming layer, Journal of Power Sources, 201 (2012) 66-71.

[19] A. Yan, M. Phongaksorn, D. Nativel, E. Croiset, Lanthanum promoted NiO–SDC anode for low temperature solid oxide fuel cells fueled with methane, Journal of Power Sources, 210 (2012) 374-380.

[20] J. Qu, W. Wang, Y. Chen, X. Deng, Z. Shao, Stable direct-methane solid oxide fuel cells with calcium-oxide-modified nickel-based anodes operating at reduced temperatures, Applied Energy, 164 (2016) 563-571.